*Clay Minerals*, (2017) **52**, 299–313

# Low-frequency electrical conductivity of aqueous kaolinite suspensions: surface conductance, electrokinetic potentials and counterion mobility

CHRISTIAN WEBER*† AND HELGE STANJEK

*Clay and Interface Mineralogy, RWTH Aachen University, Bunsenstrasse 8, 52072 Aachen, Germany*

(*Received 27 April 2017; revised 17 August 2017; Associate Editor: L. Michot*)

ABSTRACT: The low-frequency conductivity of aqueous kaolinite suspensions has been measured as a function of volume fraction and concentration of KCl, $K_2SO_4$ and $BaCl_2$, respectively. These measurements were interpreted with a theoretical model accounting for surface conductivity and particle shape. For the first time, an internally consistent data set was established by measuring all parameters necessary to solve the relevant equations. The simultaneous availability of surface conductivity, surface charge density and diffuse layer charge density permitted the estimation of counterion mobilities in the stagnant layer and a consistency check for the evaluation procedure of the conductivity experiments. In agreement with current literature results, monovalent counterions were found to have a Stern layer mobility similar to their bulk mobility, whereas the mobility of divalent counterions in this layer is reduced by a factor of ~2.

KEYWORDS: surface conductance, surface charge density, zeta potential, Stern layer mobility, cation exchange capacity, kaolinite.

Kaolinite is a very common clay mineral in highly weathered soils and many sedimentary rocks, where it may contribute significantly to sorption and cation exchange processes (Dixon, 1989; Bergaya *et al.*, 2006). Recently, the impact of kaolinite on fluid flow in porous media such as reservoir rocks gets increasing attention due to attempts to understand permeability changes in the course of enhanced oil recovery (Goldenberg *et al.*, 1993; Amirianshoja *et al.*, 2013) or to establish quantitative relationships between pore-water chemistry and electrical resistivity measurements (Choo *et al.*, 2016).

*E-mail: chris.weber@chemie.tu-freiberg.de
†Present address: Institut für Physikalische Chemie, Technische Universität Bergakademie Freiberg, 09599 Freiberg, Germany
https://doi.org/10.1180/claymin.2017.052.3.02

The structure of kaolinite ($Al_2Si_2O_5(OH)_4$) consists of a tetrahedral siloxane sheet, which shares oxygens with the octahedral Al-containing sheet. The OH groups on the bottom of the octahedral sheet bond to the siloxane sheet of the next layer (Brindley & Robinson, 1946). Although, in comparison to other clay minerals, kaolinite has a simple structure, a detailed understanding of ion adsorption and exchange mechanisms is still lacking. Controversially, even the origin of surface charge on kaolinites is discussed.

Weiss (1959) introduced the concept of a permanent negative charge which is due to isomorphous substitution of $Al^{3+}$ for $Si^{4+}$, a concept which recurs frequently in the literature (Bolland *et al.*, 1976; Bersillon *et al.*, 2003). Ma & Eggleton (1999), on the other hand, noted that "according to the principle of local charge balance, charge differences inside a crystal are not likely to be compensated far from their source, *i.e.* at the surface". Due to the absence of an interlayer

region (as in smectites, vermiculites and micas), the only conceivable cation which could compensate the deficient charge from $Al^{3+}$ in the tetrahedral sheet could be an extra proton. But no structural evidence for such a charge balance has ever been presented (Ma & Eggleton, 1999).

Schofield & Samson (1954) observed that chloride ions adsorb positively under certain experimental conditions. Those authors presumed that this adsorption takes place at the *hk*0 faces (or, in short, at the "edges"). In order to explain such features and pH-dependent cation exchange capacities, the surface charge of kaolinite is often viewed as having one permanent (negative) component stemming from the faces and one variable (pH-dependent) component that is only assigned to the edges. This view was, however, not confirmed by a very careful and detailed experimental study (Ferris & Jepson, 1975). The latter authors concluded that ion adsorption and exchange on kaolinite cannot be explained by a simple "permanent charge plus edge charge" model.

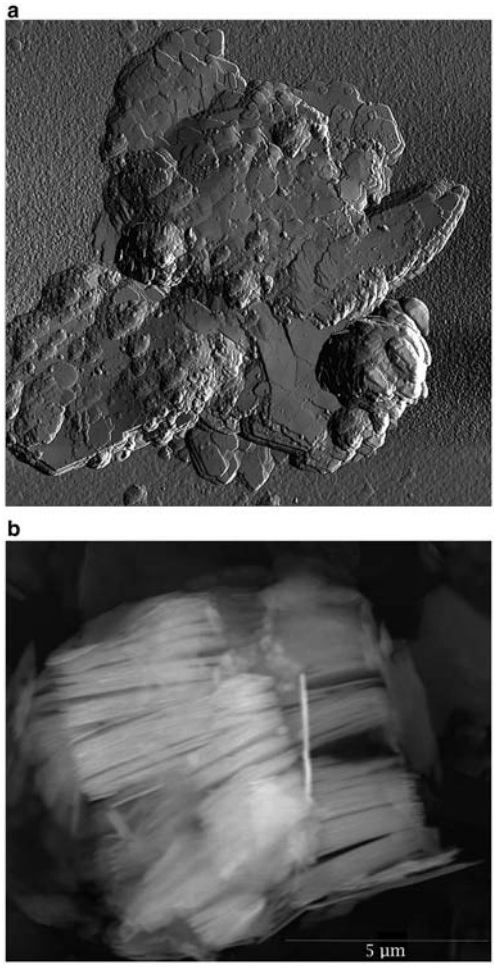


FIG. 1. (a) AFM amplitude contrast image of an individual kaolinite particle. The image is 3.8 µm × 3.8 µm in size. (b) SEM image showing a kaolinite aggregate/stack in side view.

In line with Ferris & Jepson (1975), Ma & Eggleton (1999) and Zhou & Gunter (1992) presented evidence for more complicated charging mechanisms than often envisioned for kaolinite. Those authors concluded that the basal faces are also able to protonate and can thus contribute to pH-dependent adsorption and exchange reactions. A strict geometrical distinction in terms of edge charges and face charges thus does not appear realistic. Such a picture seems plausible in view of the fact that kaolinite is a natural material that will not have atomically flat surfaces, but rather show growth steps and other "imperfections" on its basal planes (see Fig. 1).

Another important point is that the counterion surface excess (and thus cation exchange capacities) are concentration-dependent quantities. For kaolinite this has been demonstrated experimentally by Ferris & Jepson (1975) and was modeled by Vasconcelos *et al.* (2007). The latter authors predicted that counterion adsorption takes place in the inner part of the electrical double layer, increases with increasing ionic strength and depends on the type of counterion.

Apart from classical cation exchange and modelling studies, electrokinetic experiments can help to gain a better understanding of charging mechanisms and double layer structure. In clay systems, by far the most abundant technique is electrophoresis in which the electrophoretic mobility is the primary experimental parameter. This quantity is usually converted into a ζ potential by virtue of the Helmholtz-Smoluchovski theory. Apart from other limitations inherent in this theory (Delgado *et al.*, 2007), it does not account for surface conductance. Illustrative examples for the prominence of surface conductance can be found in few articles (O'Brien & Rowlands, 1993; Rowlands & O'Brien, 1995; Rasmusson *et al.*, 1997; Chassagne *et al.*, 2009). Comparing different electrokinetic techniques with conductance data, those authors concluded that part of the surface conductivity originates behind the slip plane and that the particle shape needs to be taken into account when converting electrokinetic or conductance data to electrokinetic potentials. Despite their experimental and theoretical efforts, they were not able to achieve electrokinetic

https://doi.org/10.1180/claymin.2017.052.3.02 Published online by Cambridge University Press

consistency, *i.e.* obtain the same electro-surface parameters from two independent techniques. In this regard it is important to realize two things: (1) ζ potentials are not directly measurable quantities, there is always a theoretical conversion step and the resulting electrokinetic potential will depend on the suitability of the theory used to compute it. (2) If surface conductance behind the slip plane is indeed operative, it must be incorporated in the calculation of electrokinetic potentials. This implies that the electrokinetic potential is not the only parameter that characterizes the electrical state of an interface.

On top of the surface conductance issue there may be a number of reasons why electrokinetic consistency has not been achieved in clay systems. One obvious issue might be the fact that certain properties of the particles such as their particle radius and/or aspect ratio are treated as fit parameters in some data-evaluation schemes (Rasmusson *et al.*, 1997). Though this procedure is not objectionable as such, it may mask interesting and relevant features of the double layer. Further complicating aspects include the non-spherical particle shape and the particle-size distribution, the uneven and pH-dependent charge distribution, the possibility that the particles aggregate in different arrangements, depending on pH and electrolyte concentration and the fact that the particles may have rough surfaces. Moreover, clay samples are often not pure, meaning that other mineral phases are present as well.

In summary we can state that there are many aspects that may hinder a consistent interpretation of data from electrokinetic experiments. However, little is known about which of these points, if not all, are in fact crucial in the conversion of a measured quantity into electro-surface parameters. Here we adopt a practical, guided approach and consider only some characteristics of the particles and see whether a consistent data interpretation can be achieved. These characteristics are the particle shape and surface conductance originating behind the slip plane. All parameters that are needed for solving the relevant electrokinetic equations have been determined experimentally and, whenever possible, double-checked by independent methods.

## THEORY

### *Surface conductance*

In electrokinetic studies the influence of surface conductivity ($K^{\sigma}$) is usually expressed relative to the conductivity of the equilibrium electrolyte solution by means of the dimensionless Dukhin number, *Du* (Lyklema & Minor, 1998)

$$Du = \frac{K^{\sigma}}{K^{L} l} \tag{1}$$

Here $K^{L}$ is the conductivity of the solution and $l$ the characteristic length scale of the system. The surface conductivity has two contributions: one originating in the inner part of the double layer ($K^{\sigma^i}$), and one ascribed to the diffuse part of the double layer ($K^{\sigma^d}$). Lyklema (2001) summarized the need for distinguishing between these two contributions. In terms of Dukhin numbers one may define (Delgado *et al.*, 2007)

$$Du = Du^{d} + Du^{i} = \frac{K^{\sigma^d}}{K^{L} l} + \frac{K^{\sigma^i}}{K^{L} l} \tag{2}$$

The diffuse part of the surface conductivity was studied in the 1930s by Bikerman (1935). For a symmetrical electrolyte his result is commonly written as (Lyklema & Minor, 1998):

$$K^{\sigma^d} = \frac{2F^2 z^2 c^{\infty}}{RT\kappa}\left[D_{+}(e^{-zy^{ek}/2} - 1)\left(1 + \frac{3m_{+}}{z^2}\right) + D_{-}(e^{zy^{ek}/2} - 1)\left(1 + \frac{3m_{-}}{z^2}\right)\right] \tag{3}$$

Here F is the Faraday constant, R the ideal gas constant, $T$ the temperature, $c^{\infty}$ the electrolyte concentration in the bulk, $z$ the charge of the ions (including sign), $y^{ek}$ the dimensionless electrokinetic potential ($y^{ek} = F\zeta/RT$) and κ the reciprocal Debye length, defined as

$$\kappa = \sqrt{\frac{F^2 \sum_i z_i^2 c_i^{\infty}}{RT\varepsilon\varepsilon_0}} \tag{4}$$

The dimensionless quantity $m$ is given by

$$m_{\pm} = \left(\frac{RT}{F}\right)^2 \frac{2\varepsilon\varepsilon_0}{3\eta D_{\pm}} \tag{5}$$

in which $\varepsilon_0$ is the permittivity of free space, ε the relative dielectric constant of the solvent, η its viscosity and $D_{\pm}$ the diffusion coefficient of the ionic species considered. The relevant diffusion coefficient is the self diffusion coefficient in the bulk solution, which is related to the ionic mobility *via* the Nernst-Einstein relationship.

For high negative electrical potentials, the contribution of co-ions becomes negligible and equation 3

https://doi.org/10.1180/claymin.2017.052.3.02 Published online by Cambridge University Press

can be rewritten as:

$$K_2^{\sigma^d} = \frac{2F^2 z_2^2 c^\infty}{RT\kappa}\left[D_2(e^{-z_2 y^{ek}/2} - 1)\left(1 + \frac{3m_2}{z_2^2}\right)\right] \quad (6)$$

Restricting equation 2 to cations (subscript 2) delivers (Minor *et al.*, 1998b)

$$Du_2 = Du_2^d + Du_2^i = \frac{K_2^{\sigma^d}}{K_2^L \cdot l}\left(1 + \frac{K_2^{\sigma^i}}{K_2^{\sigma^d}}\right) \quad (7)$$

in which $K_2^L$ denotes the conductivity due to counterions, which can be obtained from (Lyklema, 1991)

$$K_2^L = \frac{F^2}{RT} z_2^2 c_2^\infty D_2 \quad (8)$$

Substituting equation 6 into equation 7 provides $Du_2$ for a symmetrical electrolyte

$$Du_2 = \frac{2}{K_2^L l}\frac{F^2 z_2^2 c^\infty}{RT\kappa}\left[D_2(e^{-z_2 y^{ek}/2} - 1)\left(1 + \frac{3m_2}{z_2^2}\right)\right] \cdot \left(1 + \frac{K_2^{\sigma^i}}{K_2^{\sigma^d}}\right) \quad (9)$$

The last equation illustrates nicely that $K_2^{\sigma^i}/K_2^{\sigma^d}$ needs to be known in order to calculate $y^{ek}$ from $Du_2$. The corresponding relations for 2-1 and 1-2 electrolytes are provided in the Appendix.

### *Conductivity of suspensions consisting of oblate spheroids*

Based on the initial efforts of Dukhin & Shilov (1980), O'Brien & Ward (1988) developed a theoretical framework describing the static electrical conductivity of dilute suspensions made up of randomly oriented, mono-disperse spheroids with relatively thin double layers ($\kappa l \gg 1$). Their analytical solution, derived for two-species electrolyte solutions, was given by (O'Brien & Ward, 1988)

$$\frac{K^*}{K^L} = 1 - \varphi[f^0(0) + 2f^1(0)] - \frac{\varphi D_2 z_2^2 n_2^\infty}{\sum_{j=1}^N D_j z_j^2 n_j^\infty}[f^0(Du_2) - f^0(0) + 2\{f^1(Du_2) - f^1(0)\}] \quad (10)$$

Here $K^*$ denotes the conductivity of the suspension, $\varphi$ the volume fraction of solid and $n^\infty$ the ionic number density in the bulk solution. Counterions are indicated by subscript 2 and the summation over $j$ includes all species present in the solution. For easy reference the $f$-functions for oblate spheroids (aspect ratio $n < 1$) are collected in the Appendix. These functions describe the polarization of the particle in field-parallel (superscript 0) and field-perpendicular (superscript 1) orientation. Note that $f(0)$ means $f(Du_2 = 0)$.

Apart from field-aligned particles with $n < 0.1$ and $Du_2 < 0.05$, the analytical representation of $f^0(Du_2)$ agrees within 5% with the numerically evaluated value. For such particles O'Brien & Ward (1988) provided numerical values (see their table 1).

## MATERIALS AND METHODS

### *Sample preparation*

A kaolinite from Caminau, Saxony, Germany, was converted to homoionic forms by exposing the raw material repeatedly to 3 M and 1 M solutions of KCl and $BaCl_2$, respectively. The samples were washed in a pressure filtration with deionized water using a 0.45 μm filter. When the conductivity of the washing water fell below 2 μS/cm, the samples were re-dispersed in deionized water and freeze dried. X-ray diffraction revealed 0.81 g/g kaolinite, 0.18 g/g illite/muscovite and 0.01 g/g quartz (Weber *et al.*, 2014).

### *Measurement of electrical conductivity*

The electrical conductivities were measured with a WTW LF-3000 conductivity meter. The device adjusts its frequency depending on the conductivity of the solution between 170 Hz (20–200 μS/cm) and 400 Hz (0.2–20 mS/cm). The conductivity cell K25 from Spectronic Camspec has four carbon electrodes separated by a gap of 6 mm. The cell constant was calibrated at 25°C using 0.01, 0.1 and 1 M KCl solutions, the conductivities of which were taken from Haynes *et al.* (2012). The conductivities of all solutions were well described by a single cell constant, which indicates linearity in the potential-current response and absence of electrode polarization.

For conductivity measurements, the samples were placed in a double-walled, water-filled glass vessel connected to a water bath. Suspensions were prepared by immersing an appropriate mass of sample in 100 mL of the desired electrolyte solution. After the suspensions were stirred for some time at 25°C, the stirrer was turned off and the material was allowed to settle. After measuring the conductivity of the particle-free supernatant, a defined volume of this equilibrium

https://doi.org/10.1180/claymin.2017.052.3.02 Published online by Cambridge University Press

electrolyte was withdrawn and the conductivity of the remaining suspension was measured. Adding aliquots of the equilibrium electrolyte solution provides suspensions of varying volume fraction, but without changing the chemistry of the system. All measurements were performed at 25.0°C.

### *pH measurements*

pH measurements were performed in suspensions of 0.1 vol.% at 25°C. The electrolyte concentration was adjusted by adding dry salt (KCl or $BaCl_2$, respectively) to the suspensions. A Schott A1180 glass electrode was used in combination with a Schott B2200+ Ag/AgCl reference electrode, filled with 3 M KCl. EMF readings were taken with a Keithley 6514 electrometer with an input impedance >200 TΩ. Readings were considered stable when the voltage drift was <0.1 mV/min for several minutes. The electrodes were calibrated against secondary WTW standards of pH = 4.01, 7.0 and 10.01 at 25°C. Note that: (1) no effort was made to exclude $CO_2$ from the suspensions, as this was not done in the conductivity measurements; and (2) moderate stirring had no significant influence on the EMF measured.

### *Surface charge density*

Surface charge densities have been calculated by measuring the decrease of counterion concentration in particle-free equilibrium solutions. For this purpose, suspensions of 1.1 vol.% were prepared and left for sedimentation overnight. The counterion concentrations were determined in the equilibrium electrolyte solutions and in the initial solutions, respectively, by ion chromatography (Metrohm IC 850 professional).

The counterion surface charge density ($\sigma_2^0$) is calculated from

$$\sigma_2^0 = -z_2 F \Gamma_2 \tag{11}$$

where $\Gamma_2$ is the surface excess of counterions in mol/m$^2$. This quantity is obtained from

$$\Gamma_2 = \frac{n_i^\infty - n_e^\infty}{A} \tag{12}$$

in which $n_i^\infty$ and $n_e^\infty$ denote the number of moles in the initial and equilibrium solution, respectively. Multiplication of the specific surface area $A_{sp}$ (see below) with the mass of solid $m$ in suspension gives $A$. Concentration measurements were done in triplicate with a reproducibility of better than 1%.

### *Particle size, shape and aggregation*

Atomic force microscopy (AFM) and scanning electron microscopy (SEM) images were recorded in order to obtain a visual impression of the particle shape and surface structure of the particles. Aqueous suspensions ($\sim 4 \times 10^{-4}$ vol.%) were pipetted onto microscopic cover glasses for AFM measurements and onto metallic stubs for SEM measurements. The samples were then either dried overnight or on a heating plate.

Equivalent spherical diameters were assessed by ultrasound attenuation, laser scattering and sedimentation, respectively. The aspect ratio used in the present study was determined conductometrically in 50 mM $BaCl_2$ solutions. In contrast to earlier experiments (Weber *et al.*, 2014), the temperature was reduced to 5°C. The main idea of working at low temperature is to reduce the mobility of counterions and thereby minimize surface conductance, which is a necessary requirement for obtaining accurate aspect ratios from conductance measurements.

The absence of aggregation within the range of salt concentrations was judged from ultrasound attenuation measurements (Dispersion Technology DT1200) on suspensions of varying salt concentration.

### *Specific surface area*

Nitrogen adsorption and desorption isotherms were recorded on a Micromeritics Gemini VII at 77 K. The samples were outgassed in vacuum ($p = 2.6$ kPa) at 130°C for 12 h. BET surface areas were calculated following the recommendations of Rouquerol *et al.* (1994). In addition to BET values, surface areas were measured by column wicking experiments with n-octane. For details regarding sample preparation and the equations presented below, we refer to our earlier work (Weber & Stanjek, 2012).

In these experiments, the mass uptake ($m$) due to spontaneous imbibition is measured as a function of time ($t$). For vertically homogeneous powder packings a plot of the squared mass *vs*. time results in a linear relationship. With the assumption that n-octane completely wets the kaolinite surfaces (*i.e.* $\cos\theta = 1$) the slope of said relationship is evaluated to obtain the capillary constant C

$$C = \frac{dm^2}{dt} \cdot \frac{2\eta}{\rho^2 \gamma_{lv}} \tag{13}$$

where $\rho$ and $\eta$ are the density and viscosity of the liquid and $\gamma_{lv}$ is the surface tension of the liquid-vapour

https://doi.org/10.1180/claymin.2017.052.3.02 Published online by Cambridge University Press

interface. C is related to the effective pore radius $r_{eff}$ by

$$r_{eff} = \frac{C}{(1-\varphi)^2 A_c^2} \quad (14)$$

where $\varphi$ is the volume fraction and $A_c$ the macroscopic cross-sectional area of the powder column. Knowledge of the porosity and the solid density $\rho_s$ allows us to estimate the specific surface area $A_{sp}$ from the effective radius (White, 1982):

$$A_{sp} = \frac{2(1-\varphi)}{\varphi \rho_s r_{eff}} \quad (15)$$

## RESULTS

### *Particle size, shape and aggregation*

The SEM image (Fig. 1b) shows an aggregate/stack of kaolinite particles in side view, which illustrates the highly non-spherical shape of the particles. On the AFM scale (Fig. 1a) one observes quite irregularly shaped particles with a variety of morphological surface features such as islands, pits, steps and other particles adhering to it. The lateral dimensions of this particular particle are ~3–4 μm and depending on the position, the height of the particle is $\sim 10^1$–$10^2$ nm. Inspection of a number of particles reveal similar features. These observations underline the ill-defined nature of the sample. Treating such particles as oblate spheroids is an approximation in itself and defining an aspect ratio even for a single particle is quite ambiguous, as the lateral dimensions and corresponding heights are not homogeneous across the particle.

In order to check the accuracy of approximating the particles as oblate spheroids, three different particle sizing techniques have been used. The resulting particle-size distributions are displayed in terms of equivalent spherical diameters (esd) in Fig. 2a. The observed discrepancies between the different techniques have a physical origin: the standard evaluation schemes in particle sizing devices treat the particles as being spheres. In the case of non-spherical particles, a technique that relates the volume of a particle in a given size class to its diameter (as in acoustic spectroscopy) must result in a different esd than a technique that relates the area (as in laser scattering) of this particle to its diameter. For a given geometrical model of the particle, the different esd values are related to each other by the aspect ratio. The availability of multiple particle-size distributions and independently determined aspect ratios not only offers a way to check the aspect ratio, but also the accuracy of the underlying geometrical model.

TABLE 1. Dukhin numbers, ratios of inner- to diffuse layer-surface conductivities and ζ potentials of KCl, $K_2SO_4$ and $BaCl_2$ suspensions at 25°C.

| $c_2^\infty$ [mol/m$^3$] | $Du_2$ | $K_2^{\sigma'}/K_2^{\sigma d}$ | ζ [mV] |
|---|---|---|---|
| $K_2SO_4$, $K_2^{\sigma d} = 2.8 \cdot 10^{-10}$ S | | | |
| 1 | 0.47 | 0.8 | −45 |
| 5 | 0.29 | 4.7 | −26 |
| 10 | 0.24 | 8.5 | −20 |
| 50 | 0.20 | 38.9 | −10 |
| KCl, $K_2^{\sigma d} = 2.9 \cdot 10^{-10}$ S | | | |
| 1 | 0.48 | 0.8 | −44 |
| 5 | 0.28 | 4.1 | −25 |
| 10 | 0.24 | 7.8 | −18 |
| 50 | 0.20 | 35.6 | −9 |
| $BaCl_2$, $K_2^{\sigma d} = 6.4 \cdot 10^{-10}$ S | | | |
| 1 | 0.56 | 0.6 | −41 |
| 5 | 0.29 | 3.3 | −25 |
| 10 | 0.25 | 6.4 | −20 |
| 50 | 0.22 | 31.5 | −11 |

Figure 2b shows the particle-size distribution after recalculating the data of Fig. 2a to diameters of oblate spheroids. For these calculations we have used the conductometrically determined aspect ratio ($n = 1/27$) and the relations of Jennings & Parslow (1988) for oblate spheroids. The good agreement between the recalculated particle-size distributions in Fig. 2b shows that treating the particles as oblate spheroids with a single-valued aspect ratio is a good approximation.

Finally, note that the particle-size distributions displayed in Fig. 2 have been measured in different aqueous electrolyte solutions. Laser scattering experiments were conducted in a Na-pyrophosphate solution, which is a standard dispersant for particle sizing. Ultrasound measurements were performed in pH ≈ 10 solutions and the sedimentation analysis has been performed under unspecified conditions[1].

Because no dispersant was used in any of the conductivity experiments, ultrasound attenuation measurements were performed under the relevant conditions, *i.e.* similar volume fractions and 1–50 mM KCl

[1]These values are taken from the materials' data sheet, established in a round-robin and documented by the Ernst-Moritz-Arndt University Greifswald in 1987. The document is available on request from the authors.

https://doi.org/10.1180/claymin.2017.052.3.02 Published online by Cambridge University Press

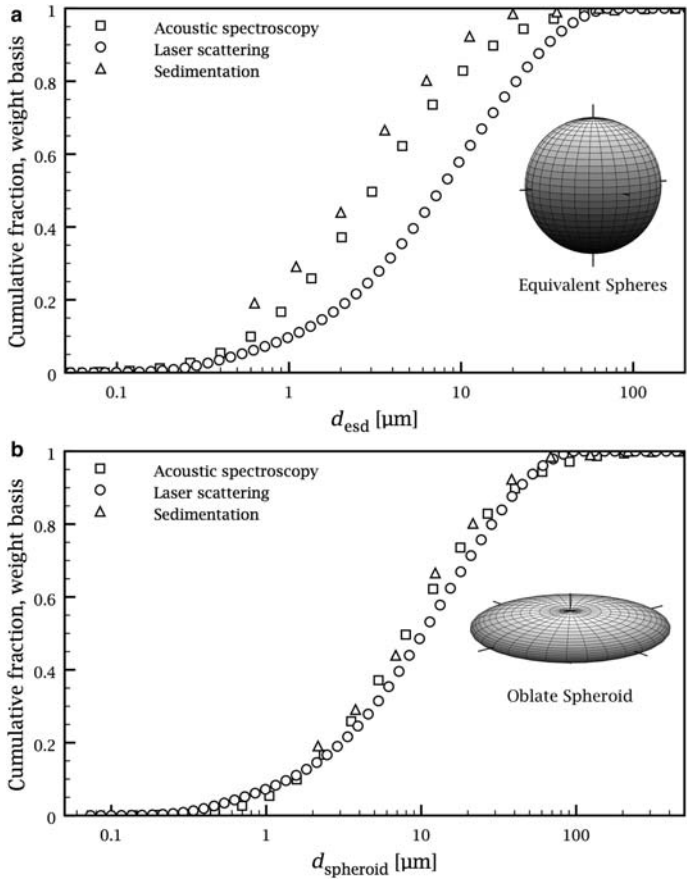


FIG. 2. Cumulative particle-size distributions from different experimental techniques: (a) equivalent spherical diameters; (b) recalculated major diameters of oblate spheroids using the conductometrically determined aspect ratio. Note that the aspect ratio of the inset in part b is not to scale.

and $BaCl_2$, respectively. No difference was noted in the particle-size distribution shown in this section. These results provide good evidence that no electrolyte-induced aggregation takes place, which allows us to use the same aspect ratio and particle size for all calculations to follow.

### *Specific surface area*

In terms of IUPAC nomenclature (Thommes *et al.*, 2015), nitrogen ad-/desorption isotherms were of type 2 with a minimal hysteresis loop of type H3. Application of the BET equation with a molecular cross section of 0.162 $nm^2$ gave a specific surface area of $15.5 \pm 0.03$ $m^2/g$.

The volume fraction in equation 15 has been estimated from the amount of kaolinite ($\rho_s$ = 2,630 $kg/m^3$) weighed in a given volume and from the amount of liquid taken up by the column. Both approaches provided a similar volume fraction of $\varphi = 0.247 \pm 0.004$. Three replicate measurements resulted in a specific surface area of $15.4 \pm 0.1$ $m^2/g$, in agreement with the gas adsorption result. Note that reasonable agreement between surface areas from gas adsorption and from negative adsorption of co-ions was observed for kaolinites (Schofield & Samson, 1954).

### *Surface charge density*

For Ba- and K-kaolinite, the surface charge densities $\sigma_2^0$ (*cf.* equation 11) increase linearly with increasing bulk concentrations (Fig. 3) and the intercepts of both regression lines do not differ from zero. The Ba-saturated sample shows far greater charge densities

https://doi.org/10.1180/claymin.2017.052.3.02 Published online by Cambridge University Press

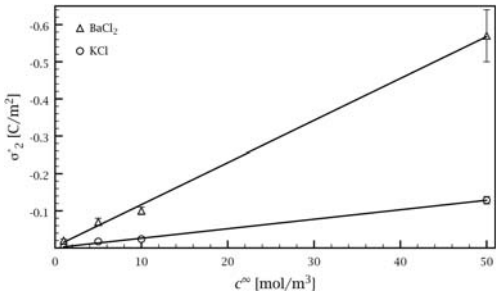


FIG. 3. Counterion surface-charge density as a function of electrolyte concentration. Error bars result from three replicate measurements and lines show a linear regression through the data.

than the K-saturated one. Further, it is important to note that the pH of the suspensions is between 5.5 and 5.6, independent of the electrolyte.

### *Electrical conductivity*

The conductivity ratio $K^*/K^L$ is linear in volume fraction and intercepts at $K^*/K^L = 1$ for $\varphi = 0$ (Fig. 4). $K_2SO_4$ and $BaCl_2$ suspensions have been studied at approximately half volume fraction as compared to KCl suspensions due to the lack of material.

The slope of the $K^*/K^L(\varphi)$ relation is close to zero for the smallest counterion concentration, where the systems are close to their isoconductive point. For higher concentrations the slopes increase to reach an electrolyte-independent value at 50 mol/m$^3$.

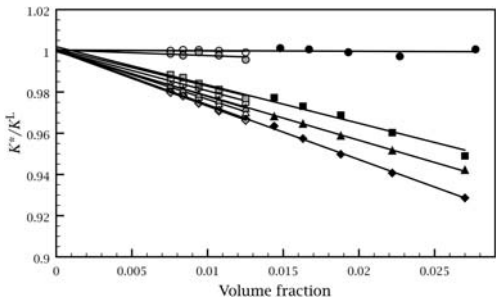


FIG. 4. Ratio of suspension conductivity to the conductivity of the equilibrium electrolyte solution as a function of volume fraction at 25°C. Grey symbols denote K-kaolinite in $K_2SO_4$; open symbols denote Ba-kaolinite in $BaCl_2$; and black symbols denote K-kaolinite in KCl, respectively. The counterion concentration is 1 mol/m$^3$ (circles), 5 mol/m$^3$ (squares), 10 mol/m$^3$ (triangles) and 50 mol/m$^3$ (diamonds).

As a first step in the data evaluation, $Du_2$ was calculated from equation 10. The Dukhin numbers obtained represent averages of five individual measurements with standard deviations of ~±0.01. For these calculations, and those to follow, the negative adsorption of co-ions was ignored. This can be justified by considering that the surface area of kaolinite is quite small and the volume of the suspension is large.

Diffusion coefficients valid at infinite dilution were used (Haynes *et al.*, 2012). Because ionic diffusion coefficients are concentration-dependent quantities, typically decreasing by a few per cent in the concentration range studied here, a comparison with concentration-dependent diffusion coefficients was made (Chhih *et al.*, 1994). The diffusion coefficients were calculated at the corresponding bulk concentration and no significant changes in the results were observed.

A plot of $Du_2$ *vs.* $1/K_2^L$ (see Fig. 5) shows a striking linearity and a non-zero intercept for $1/K_2^L \rightarrow 0$. At low electrolyte concentrations, in particular, Dukhin numbers were observed to be greater for $Ba^{2+}$ than for $K^+$. To gain an understanding of the significance of the observed linearity, we rewrite equation 7 as:

$$Du_2 = \frac{K_2^{\sigma^d}}{l} \cdot \frac{1}{K_2^L} + Du_2^i \qquad (16)$$

This equation suggests that the slope of the linear relation shown in Fig. 5 is given by $K_2^{\sigma^d}/l$, which is independent of electrolyte concentration. The motivation for writing equation 16 in this specific form derives from the fact that electrical double layers become more and more non-diffuse as the concentration of the supporting electrolyte is increased. This is captured in the constant $Du_2^i$-term, which implies that

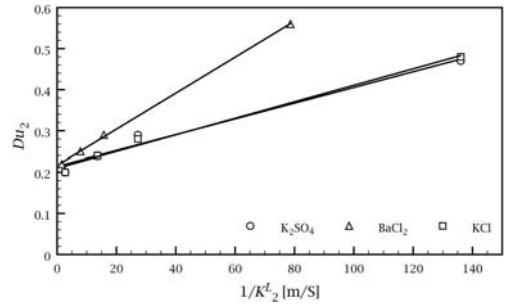


FIG. 5. $Du_2$ as a function of $1/K_2^L$ at 25°C, electrolyte indicated. Symbols represent experimental points and lines are linear regressions.

https://doi.org/10.1180/claymin.2017.052.3.02 Published online by Cambridge University Press

$K_2^{\sigma^i}$ is a linearly increasing function of bulk electrolyte concentration. In relation to a concentration-independent ionic mobility in the inner part of the double layer (see below), the linearity of $K_2^{\sigma^i}$ suggests a linear Stern layer adsorption isotherm.

To quanitfy the individual components of the surface conductivity, a discussion about the characteristic length, $l$, is in order, and this is provided below.

## DISCUSSION

### *Particle size and associated parameters*

The particle-size distribution of the Caminau kaolinite shows a considerable spread over two orders of magnitude (Fig. 2), which invokes the question about how this spread affects electro-surface parameters. As long as $\kappa l \gg 1$, the $\zeta$ potential, the diffuse-layer charge density and the diffuse contribution to the surface conductivity will be independent of particle size. Moreover, the measured surface-charge density is a single-valued number, representing an average over all particle sizes. From the overall electroneutrality of electrical double layers, we can conclude that $\sigma^i$ should be single valued as well. The same will then be true regarding the inner-layer surface conductance. As the experimental Dukhin number represents an average over all particle sizes, it appears reasonable to use a single characteristic length.

Here, the dimensions derived from the aspect ratio ($n = 1/27$) and the $d_{50}$ of the cumulative distribution of Fig. 2b are used. The maximum cross-sectional radius normal to the axis of revolution is thus $a =$ 3.97 μm and along the axis of revolution $b =$ 0.147 μm. But which length has to be used as the characteristic length $l$ in all equations above? Different authors define the characteristic length differently without apparent reasoning for their choice. O'Brien & Ward (1988) define $l$ as the dimension of the larger semi-axis, whereas Chassagne & Bedeaux (2008) define $l$ as the dimension of the short semi-axis of an oblate spheroid. In discussing relaxation times of charged, non-spherical particles subject to an external electrical field, Jiménez & Bellini (2010) stated that the characteristic length may be a suitable combination of the dimensions of the spheroid's principal axes. From a perspective of electrokinetic radii (the product $\kappa l$), it would be logical to use the dimension of the short semi-axis, because this is the limiting factor for the applicability of most theoretical frameworks. Using the above-mentioned lengths for $a$ and $b$ and $c_2^\infty = 1$ mM, the Caminau kaolinite would have "average" electrokinetic radii of $\kappa b = 15$ and $\kappa a = 413$ for the 1-1 electrolyte, $\kappa b = 27$ and $\kappa a = 715$ for the 2-1 electrolyte, and $\kappa b = 19$ and $\kappa a = 506$ for the 1-2 electrolyte, respectively.

The 1-1 electrolyte situation, in particular, comes close to the condition $\kappa b \gg 1$ of a "flat double layer", for which the Bikerman (1935) and the O'Brien and Ward (1988) theory was derived. A modification of the theory to small electrokinetic radii would require a solution of the Poisson-Boltzmann and electrokinetic equations in spheroidal geometry. Although efforts in this direction have been taken (Chassagne & Bedeaux, 2008), this particular theory is limited to electrolytes of equal diffusion coefficients.

Given the drastic modifications needed to create a sufficiently general theory, and the questionable meaning of surface excess conductivity at radii close to $\kappa^{-1}$, we will accept the resulting uncertainties from the flat double layer approximations.

### *Characteristic length*

To judge whether $a$ or $b$ needs to be identified with $l$, the following approach is used:

(1) Calculate the total surface conductivity from $Du_2$ using either $a$ or $b$ as $l$
(2) Calculate $K_2^{\sigma^d}$ from the slope of the $Du_2$ *vs.* $1/K_2^L$ relations, again using either $a$ or $b$ as $l$
(3) Obtain $K_2^{\sigma^i}$ as the difference between $K_2^\sigma$ and $K_2^{\sigma^d}$.

To decide which length scale is relevant, the surface conductivity needs to be compared with the experimental surface charge density. Expressing the total surface conductivity in terms of charge densities and ionic mobilities results in:

$$K_2^\sigma = u_2^i \sigma_2^i + u_2^\infty \left(1 + \frac{3m_2}{z_2^2}\right)\sigma_2^d \qquad (17)$$

where $u_2^i$ is the mobility of counterions in the stagnant layer and $u_2^\infty$ their bulk mobility. The condition of electroneutrality $\sigma_2^0 + \sigma_2^i + \sigma_2^d = 0$ provides, then, in combination with equation 17, the following relation:

$$K_2^\sigma = -u_2^i \sigma_2^0 + \left[\left(1 + \frac{3m_2}{z_2^2}\right)u_2^\infty - u_2^i\right]\sigma_2^d \qquad (18)$$

This relation was used by Löbbus *et al.* (2000) to estimate stagnant layer mobilities and shows that a plot of $K_2^\sigma$ *vs.* $\sigma_2^0$ should result in a straight line with slope

https://doi.org/10.1180/claymin.2017.052.3.02 Published online by Cambridge University Press

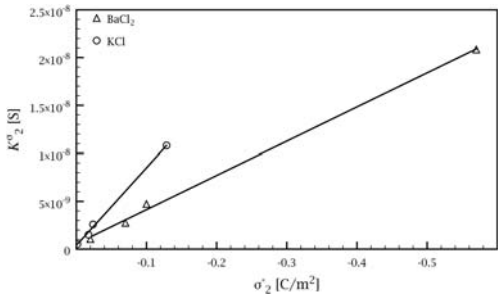


FIG. 6. $K_2^{\sigma}$ as a function of $\sigma_2^0$ at 25°C, calculated with $l = b$. Symbols represent experimental points and lines, linear regressions.

$-u_2^i$ and an intercept that is proportional to $\sigma_2^d$. The critical parameters for deciding whether $a$ or $b$ needs to be defined as the characteristic length are values for the stagnant layer mobility.

Figure 6 shows a plot of the surface conductivity (calculated with $l = b$) as a function of surface charge density for KCl and $BaCl_2$ suspensions. The stagnant layer mobilities, expressed relative to the bulk mobility, are $u_K^i/u_K^\infty = 1.06 \pm 0.04$ and $u_{Ba}^i/u_{Ba}^\infty = 0.54 \pm 0.02$. Though our Ba mobility ratio is somewhat lower than usually found for divalent ions, the values are in good agreement with stagnant layer mobilities reported in the literature (Lyklema & Minor, 1998; Minor *et al.*, 1998a,b; Löbbus *et al.*, 2000; Lyklema, 2001, 2002, 2003; Jiménez *et al.*, 2005). The second choice of $a = l$ leads to mobility ratios in the stagnant layer of ~27 for potassium and ~14 for barium. It is therefore the dimension of the short semi-axis, which results in physically sound mobilities.

## *Diffuse layer charge density*

Having identified the characteristic length scale for our system, the values of $Du_2$, $K_2^{\sigma^d}$ and $K_2^{\sigma^i}$ are used to extract the electrokinetic potential from equation 9 for symmetrical electrolytes and the corresponding relations given in the Appendix for the asymmetrical electrolytes. For the symmetrical case, the counterion component of the diffuse layer charge density of a flat double layer can then be calculated from (Lyklema, 1995):

$$\sigma_2^d = \sqrt{2\varepsilon\varepsilon_0 RTc^\infty}[e^{-zy^d/2} - 1] \qquad (19)$$

Here $y^d$ is the dimensionless electrical potential at the outer Helmholtz plane which will be set identical to the dimensionless electrokinetic potential. For a general discussion on this "identity" see studies by Hunter (1981) and Lyklema (2011) and for the kaolinite-aqueous solution system see Hunter & Alexander (1963a,b).

As a consistency check, $\sigma_2^d$ computed from the conductivity data can be compared with the value calculated from the linear regression of the data in Fig. 6. Note that these two data evaluation schemes are independent. Electrokinetic potentials, and thus $\sigma_2^d$, depend on the ratio of inner- to diffuse layer-surface conductivity, which is obtained from equation 16. The diffuse layer charge density obtained from the regression on the other hand, depends only on the total surface conductivity and the surface-charge density, which is determined independently.

Regarding the KCl samples, we obtain (all values in $\mu C/cm^2$) $\sigma_2^d(cond.) = 0.25 \pm 0.02$ and $\sigma_2^d(reg.) = 0.32 \pm 0.15$; for the $BaCl_2$ samples $\sigma_2^d(cond.) = 0.75 \pm 0.01$ and $\sigma_2^d(reg.) = 1.0 \pm 0.7$. Taking into account the large number of experimental parameters (surface area, surface charge density, particle size and distribution, aspect ratio and conductivity) and the possible errors inherent in their experimental determination, this agreement is very encouraging.

## *General discussion*

Table 1 shows the Dukhin number, electrokinetic potential (equation 9 and those in the Appendix) and the ratio of inner- to diffuse layer surface conductivity obtained from equation 16. The correspondence of all parameters for KCl and $K_2SO_4$ at similar counterion concentration shows that the approximations made in the theoretical section, *i.e.* ignoring the co-ion contributions, were reasonable for our systems. This is a requirement for the application of equation 10 and allows further data interpretation. The fact that essentially identical electrokinetic potentials were obtained regardless of the cationic charge may be fortuitous, but for further conclusions, other monovalent and divalent ions should be studied. At this point it is stressed that treating the surface conductivity as entirely diffuse (*i.e.* ignoring the $(1 + K_2^i/K_2^d)$ term in equation 9) would have resulted in electrokinetic potentials that, in terms of absolute numbers, increase with increasing electrolyte concentration.

From the ratio $K_2^{\sigma^i}/K_2^{\sigma^d}$ it is evident that the diffuse layer contribution dominates slightly at $c_2^\infty = 1$ mM. The increase in $K_2^{\sigma^i}/K_2^{\sigma^d}$ with increasing electrolyte concentration shows that the double layer becomes increasingly non-diffuse under these conditions, meaning that the surface-charge density is more compensated in the non-diffuse part of the double layer than in the diffuse one. This is in line with the

https://doi.org/10.1180/claymin.2017.052.3.02 Published online by Cambridge University Press

modeling results of Vasconcelos *et al.* (2007) mentioned in the introduction. Given the quoted stagnant-layer ionic mobility, the non-diffuse nature of the double layer results in a substantial surface conductivity that mainly originates behind the slip-plane.

The significance of surface conductance in clay-systems has already been realized by Lorenz (1969) and Swartzen-Allen & Matijević (1974) mentioned several references stressing the importance of Stern layers. Evidence for the importance of counterions residing in the Stern layer can also be deduced from the large low-frequency dielectric increment often reported for kaolinite and other clay minerals (Arulanandan & Mitchell, 1968; Lockhart, 1980; Arroyo *et al.*, 2000; Ishida *et al.*, 2000).

Considering the huge theoretical efforts that have been made in developing electrokinetic theories for non-spherical particles, it is surprising that the great majority of electrokinetic experiments on clay minerals use the simple Helmholtz-Smoluchovski theory. Exceptions (O'Brien & Rowlands, 1993; Rowlands & O'Brien, 1995; Rasmusson *et al.*, 1997; Chassagne *et al.*, 2009) stress the importance of accounting for surface conductivity, especially for stagnant layer conductivity. But even in these advanced studies the authors did not obtain electrokinetic consistency. Apart from the difficulty of accounting properly for stagnant layer conductivity, the reasons for this are not entirely clear. Some points to note are: (1) experiments were interpreted on the basis of equivalent spherical diameters and, depending on the experimental technique, these were used as adjustable parameters; (2) aspect ratios were guessed or used as fit parameters; (3) the long semi-axis was used as the characteristic length, which in connection with the use of equivalent spherical diameters is somewhat inconsistent. These points hinder a direct comparison of our results with those of the aforementioned articles. Note that the $\zeta$ potentials obtained by O'Brien & Rowlands (1993) and Rowlands & O'Brien (1995) are far greater than those reported here. Apart from differences in pH, the choice of the characteristic length may be responsible for this discrepancy. Had we used the long semi-axis for further interpretation, $\zeta$ potentials of comparable magnitude would have been obtained, but then at the expense of obtaining unrealistically high stagnant layer mobilities and a strong disagreement between $\sigma_2^d(reg.)$ and $\sigma_2^d(cond.)$.

Finally the present authors wish to comment on the estimate of stagnant layer mobility made by Rowlands & O'Brien (1995) and Rasmusson *et al.* (1997). Those authors estimated a ratio of inner-layer to bulk mobility of 0.56 and 0.6 for Na on kaolinite and smectite, respectively. Their argument may be summarized as follows: the diffuse layer charge densities obtained from dielectric response measurements ($\sigma_{DR}$) were greater than those obtained from (dynamic) mobility measurements ($\sigma_{Mob}$). They go on to argue that $\sigma_{DR}$ is likely to have a contribution from stagnant layer ions whereas their influence would not necessarily be reflected in $\sigma_{Mob}$. The mobility ratio was then estimated from

$$\sigma_{DR} = \sigma_{Mob} + \delta_{St}\sigma_{St}$$

where $\delta_{St}$ denotes the ratio of stagnant layer to bulk mobility and $\sigma_{St}$ is our $\sigma^i$. The Stern layer charge is then estimated as $-\sigma^0 = \sigma_{St} + \sigma_{Mob}$, in which $\sigma^0$ is determined from the cation exchange capacity. This last step is the problematic one because cation exchange capacities[2] are frequently determined at high concentrations of the index cation, except methods based on high selectivity such as the Cu-Trien method (Stanjek & Künkel, 2016). The reasoning for high concentrations is to shift the exchange reaction to the right as far as possible and then the amount of exchanged cations would reflect the isomorphous substitution in the crystal structure. However, considering the results in Fig. 3 and older literature on clay minerals (Jenny, 1932, 1936; Ferris & Jepson, 1975; Weiss, 1959) the counterion surface excess (and thus cation exchange capacities and surface charge densities) are electrolyte-concentration dependent quantities for these systems. It is therefore not precluded that the surface charge density used by Rowlands & O'Brien, 1995 and Rasmusson *et al.* (1997) is overestimated, at least for the lower concentration range. Lower surface-charge densities would correspond to greater mobility ratios in their calculations.

The little experimental evidence available on the inner part of the double layer in clay systems points towards a stagnant layer mobility that is of the same order of magnitude as bulk mobilities. Such experimental estimates of stagnant layer mobilities are very useful in geophysical models, where their order of magnitude is debated intensively (Revil, 2012, 2014; Weller *et al.*, 2013).

[2]Though cation exchange capacities are used routinely as key quantities in the characterization of clay minerals, the term is quite improperly defined. Some authors acknowledge the dependence on external parameters such as temperature and solution composition, while others describe it as a property of the solid that is independent of external parameters.

https://doi.org/10.1180/claymin.2017.052.3.02 Published online by Cambridge University Press

## SUMMARY AND CONCLUSION

It has been shown that it is essential to include the particle shape and surface conductance originating behind the slip plane in the interpretation of conductivity experiments. Regarding the quantitative estimation of surface conductance, electrokinetic potentials and charge densities, it is essential to identify the relevant length scale of the system. From a correlation of surface charge density and surface conductance, it was shown that the dimension of the small semi-axis is the relevant length scale of the studied system. The comparison of diffuse layer charge densities obtained from the aforementioned correlation and independently evaluated conductivity experiments shows that low-frequency conductivity measurements can be interpreted with internal consistency and that a distinction between inner- and diffuse layer-surface conductivity can be made.

The simultaneous availability of surface charge density and surface conductance allows us to estimate tangential counterion mobilities in the inner part of the double layer. While potassium retains its bulk mobility in the Stern layer, barium shows about half of its bulk mobility in this layer. Both values are in good agreement with literature data and help to constrain these parameters, *e.g.* in induced polarization models. Furthermore, this work highlights that kaolinite (and probably other clay minerals) do not behave very differently from other solids in this respect.

The consistency of the data interpretation suggests that many of the complicating features mentioned in the introduction are not critical in the evaluation of conductance experiments. However, the present authors are cautious in terms of generalizing with such a statement. Firstly, the pH dependency has not been studied yet and other electrokinetic experiments, especially ac-techniques, may reveal new features that are simply hidden in dc-techniques. As the results presented herein provide a good starting point, a comparison to ac-techniques such as electroacoustics would be very welcome.

## ACKNOWLEDGEMENTS

Chrsitian Weber is pleased to acknowledge helpful discussions with A. Delgado and his group. Hans Lyklema is acknowledged warmly for fruitful discussions and for reading an early version of the manuscript. Quingyun Hu is thanked for helping with the AFM measurements.

## APPENDIX

### *Ionic components of diffuse layer charge density, surface conductance and Dukhin numbers for 1-2 and 2-1 electrolytes*

Analytical solutions for the components of the diffuse layer charge density and surface conductivity of asymmetric electrolytes can only be obtained for the cases of 2-1 and 1-2 electrolytes. The expressions relevant to the present document will be presented in the following. They were derived from the "non-specific adsorption coefficients" of Grosse (2009). These are the ionic components of the surface excess and relate to the ionic components of the diffuse layer charge density by $\sigma_2^d = z_2 F \Gamma_2^d$. For a definition of symbols the reader is referred to the theoretical section of the main text.

For 1-2 electrolytes $\sigma_2^d$ is given by:

$$\sigma_2^d = \frac{6Fc^\infty}{\kappa} \cdot \frac{e^{-y^{ek}/2}\sqrt{e^{y^{ek}}+2}-\sqrt{3}}{\sqrt{3}} \tag{20}$$

Using

$$K_2^{\sigma^d} = u_2^\infty \left(1+\frac{3m_2}{z_2^2}\right)\sigma_2^d \tag{21}$$

we obtain

$$K_2^{\sigma^d} = \frac{6F^2c^\infty}{RT\kappa}\left[D_2 \frac{e^{-y^{ek}/2}\sqrt{e^{y^{ek}}+2}-\sqrt{3}}{\sqrt{3}}\left(1+\frac{3m_2}{z_2^2}\right)\right] \tag{22}$$

and

$$Du_2 = \frac{6}{K_2^L l}\frac{F^2c^\infty}{RT\kappa}\left[D_2 \frac{e^{-y^{ek}/2}\sqrt{e^{y^{ek}}+2}-\sqrt{3}}{\sqrt{3}}\left(1+\frac{3m_2}{z_2^2}\right)\right] \times \left(1+\frac{K_2^{\sigma^i}}{K_2^{\sigma^d}}\right) \tag{23}$$

By similar reasoning we find for 2-1 electrolytes:

$$\sigma_2^d = \frac{6Fc^\infty}{\kappa} \cdot \frac{e^{-y^{ek}/2}\sqrt{e^{-y^{ek}}+2}-\sqrt{3}}{\sqrt{3}}, \tag{24}$$

$$K_2^{\sigma^d} = \frac{12F^2c^\infty}{RT\kappa}\left[D_2 \frac{e^{-y^{ek}/2}\sqrt{e^{-y^{ek}}+2}-\sqrt{3}}{\sqrt{3}}\left(1+\frac{3m_2}{z_2^2}\right)\right] \tag{25}$$

https://doi.org/10.1180/claymin.2017.052.3.02 Published online by Cambridge University Press

and

$$Du_2 = \frac{12\ \mathrm{F}^2 c^{\infty}}{K_2^L l \mathrm{R} T \kappa}\left[D_2 \frac{e^{-y^{ek}/2}\sqrt{e^{-y^{ek}}+2}-\sqrt{3}}{\sqrt{3}}\left(1+\frac{3m_2}{z_2^2}\right)\right] \times \left(1+\frac{K_2^{\sigma'}}{K_2^{\sigma d}}\right) \quad (26)$$

The general procedure for calculating $y^{ek}$ for the non-symmetrical electrolytes is the same as for the symmetrical case which is described in the main text above, the only difference being that equations 23 and 26 were solved by a least-squares procedure.

## *f-Functions of equation 10*

The following equations summarize the *f* functions[3] to be used in equation 10 (O'Brien & Ward, 1988):

$$f^0(Du_2) = \frac{-Du_2 \sinh(\xi_0) K_1 - 2/3}{3\sinh(\xi_0)\cosh^2(\xi_0)[(2/3)iQ'_1 - Du_2 Q_1 K_1]} \quad (27)$$

in which $Q_1$ is the Legendre function of the first kind, evaluated at $x = i\sinh(\xi_o)$

$$Q_1(x) = \frac{x}{2}\ln\left(\frac{x+1}{x-1}\right) - 1 \quad (28)$$

and $Q'_1$ its derivate with respect to $x$. $f^0(0)$ is obtained by setting $Du_2 = 0$.

$K_1$ and $f^1(Du_2)$ are found from

$$K_1 = \left(\frac{\sinh^2(\xi_0)}{2}+1\right)\ln\left(\frac{\cosh(\xi_0)+1}{\cosh(\xi_0)-1}\right) - \cosh(\xi_0) \quad (29)$$

and

$$f^1(Du_2) = \frac{-8/3\sinh(\xi_0) + 2Du_2\cosh^2(\xi_0)K_2}{3\sinh(\xi_0)\cosh^3(\xi_0)[(4/3)i(Q_1^1)' - Du_2 Q_1^1 K_2]} \quad (30)$$

where $Q_1^1$ is the associated Legendre function of the first kind given by:

$$Q_1^1(x) = \frac{\sqrt{x^2-1}}{2}\ln\left(\frac{x+1}{x-1}\right) - \frac{x}{\sqrt{x^2-1}} \quad (31)$$

As above, $(Q_1^1)'$ is the derivate with respect to $x = i\sinh(\xi_0)$ and $f^1(0) = f^1(Du_2 = 0)$.

$K_2$ is obtained from

$$K_2 = (\cosh(\xi_0) + \cosh^{-1}(\xi_0)) - \frac{\sinh^2(\xi_0)}{2}\left(\frac{\sinh(\xi_0)}{\cosh(\xi_0)}\right)^2 \cdot \ln\left(\frac{\cosh(\xi_0)+1}{\cosh(\xi_0)-1}\right) \quad (32)$$

and for an oblate spheroid

$$\xi_0 = \frac{1}{2}\ln\left(\frac{1+n}{1-n}\right) \quad (33)$$

where $n$ is the aspect ratio.

[3]Note that the minus sign is missing in O'Brien and Ward's expression for $f^0(Du_2)$.

## REFERENCES


Amirianshoja T., Junin R., Idris A.K. & Rahmani O. (2013) A comparative study of surfactant adsorption by clay minerals. *Journal of Petroleum Science and Engineering*, **101**, 21–27.

Arroyo F.J., Carrique F., Jiménez-Olivares M.L. & Delgado A.V. (2000) Rheological and electrokinetic properties of sodium montmorillonite suspensions. II Low-frequency dielectric dispersion. *Journal of Colloid and Interface Science*, **229**, 118–122.

Arulanandan K. & Mitchell J.K. (1968) Low frequency dielectric dispersion of clay-water-electrolyte systems. *Clays and Clay Minerals*, **16**, 337–351.

Bergaya F., Lagaly G. & Vayer M. (2006) Cation and anion exchange. Pp. 979–1001 in: *Handbook of Clay Science* (F. Bergaya, B.K.G. Theng & G. Lagaly, editors). Elsevier, Amsterdam.

Bersillon J.-L., Villieras F., Michot L. & Cases J.-M. (2003) A new way of assessing clay cation adsorption using normalized salt concentration. *Clay Minerals*, **38**, 233–242.

Bikerman J.J. (1935) Die Oberflächenleitfähigkeit und ihre Bedeutung. *Kolloid Zeitschrift*, **72**, 100–108.

Bolland M.D.A., Posner A.M. & Quirk J.P. (1976) Surface charge on kaolinites in aqueous suspension. *Australian Journal of Soil Research*, **14**, 197–216.

Brindley G. & Robinson K. (1946) The structure of kaolinite. *Mineralogical Magazine*, **27**, 242–253.

Chassagne C. & Bedeaux D. (2008) The dielectric response of a colloidal spheroid. *Journal of Colloid and Interface Science*, **326**, 240–253.

Chassagne C., Mietta F. & Winterwerp J.C. (2009) Electrokinetic study of kaolinite suspensions. *Journal of Colloid and Interface Science*, **336**, 352–359.

Chhih A., Turq P., Bernard O., Barthel J.M.G. & Blum L. (1994) Transport coefficients and apparent charges of concentrated electrolyte solutions – Equations for


https://doi.org/10.1180/claymin.2017.052.3.02 Published online by Cambridge University Press

practical use. *Berichte der Bunsengesellschaft für Physikalische Chemie*, **98**, 1516–1525.

Choo H., Song J., Lee W. & Lee C. (2016) Effects of clay fraction and pore water conductivity on electrical conductivity of sand-kaolinite mixed soils. *Journal of Petroleum Science and Engineering*, **147**, 735–745.

Delgado A.V., Gonzalez-Caballero F., Hunter R., Koopal L.K. & Lyklema J. (2007) Measurement and interpretation of electrokinetic phenomena. *Journal of Colloid and Interface Science*, **209**, 194–224.

Dixon J.B. (1989) Kaolin and serpentine group minerals. Pp. 467–525 in: *Minerals in Soil Environments* (J.B. Dixon & S. Weed, editors). Soil Science Society of America, Madison, Wisconsin, USA.

Dukhin S.S. & Shilov V.N. (1980) Kinetic aspects of elctrochemistry of disperse systems. Part II. Induced dipole moment and the non-equilibrium double layer of a colloid particle. *Advances in Colloid and Interface Science*, **13**, 153–195.

Ferris A.P. & Jepson W.B. (1975) The exchange capacities of kaolinite and the preparation of homoionic clays. *Journal of Colloid and Interface Science*, **51**, 245–259.

Goldenberg L.C., Hutcheon I., Wardlaw N. & Melloul A.J. (1993) Rearrangement of fine particles in porous media causing reduction of permeability and formation of preferred pathways of flow: Experimental findings and a conceptual model. *Transport in Porous Media*, **13**, 221–237.

Grosse C. (2009) Generalization of a classic thin double layer polarization theory of colloidal suspensions to electrolyte solutions with different ion valences. *Journal of Physical Chemistry B*, **113**, 8911–8924.

Haynes W.M., Lide D.R. & Bruno T.J., editors (2012) *Handbook of Chemistry and Physics*. 93rd edition, CRC Press, Boca Raton, Florida, USA.

Hunter R. (1981) Zeta potential in colloid science – principles and applications. Pp. 1–386 in: *Colloid Science: A Series of Monographs* (R.H. Ottewill & R.L. Rowell, editors). Academic Press, London.

Hunter R. & Alexander A.E. (1963a) Surface properties and flow behavior of kaolinite Part I: Electrophoretic mobility and stability of kaolinite sols. *Journal of Colloid Science*, **18**, 820–832.

Hunter R. & Alexander A.E. (1963b) Surface properties and flow behavior of kaolinite Part II: Electrophoretic studies of anion adsorption. *Journal of Colloid Science*, **18**, 833–845.

Ishida T., Makino T. & Wang C. (2000) Dielectric-relaxation spectroscopy of kaolinite, montmorillonite, allophane and imogolite under moist conditions. *Clays and Clay Minerals*, **48**, 75–84.

Jennings B.R. & Parslow K. (1988) Particle size measurement: The equivalent spherical diameter. *Proceedings of the Royal Society of London A: Physical, Mathematical and Engineering Sciences*, **419**, 137–149.

Jenny H. (1932) Studies on the mechanism of ionic exchange in colloidal aluminum silicates. *The Journal of Physical Chemistry*, **36**, 2217–2258.

Jenny H. (1936) Simple kinetic theory of ionic exchange. I Ions of equal valency. *Journal of Physical Chemistry*, **40**, 501–517.

Jiménez M.L. & Bellini T. (2010) The electrokinetic behavior of charged non-spherical colloids. *Current Opinion in Colloid and Interface Science*, **15**, 131–144.

Jiménez M.L., Arroyo F.J., Carrique F., Kaatze U. & Delgado A.V. (2005) Determination of stagnant layer conductivity in polystyrene suspensions: temperature effects. *Journal of Colloid and Interface Science*, **281**, 503–509.

Löbbus M., van Leeuwen H.P. & Lyklema J. (2000) Streaming potentials and conductivities of latex plugs. Influence of the valency of the counterion. *Colloids and Surfaces A: Physicochemical and Engineering Aspects*, **161**, 103–113.

Lockhart N.C. (1980) Electrical properties and the surface characteristics and structure of clays II. Kaolinite – a non-swelling clay. *Journal of Colloid and Interface Science*, **74**, 520–529.

Lorenz P.B. (1969) Surface conductance and electrokinetic properties of kaolinite beds. *Clays and Clay Minerals*, **17**, 223–231.

Lyklema J. (1991) Transport phenomena in interface and colloid science. Pp. 6.1–6.97 in: *Fundamentals of Interface and Colloid Science* (J. Lyklema, editor). Academic Press, San Diego, California, USA.

Lyklema J. (1995) Electric double layers. Pp. 3.1–3.232 in: *Fundamentals of Interface and Colloid Science* (J. Lyklema, editor). Academic Press, San Diego, California, USA.

Lyklema J. (2001) Surface conduction. *Journal of Physics: Condensed Matter*, **13**, 5027–5034.

Lyklema J. (2002) Specificity in the statics and dynamics of surface-confined ions. *Molecular Physics*, **100**, 3177–3185.

Lyklema J. (2003) Lyotropic sequences in colloid stability revisited. *Advances in Colloid and Interface Science*, **100–102**, 1–12.

Lyklema J. (2011) Surface charges and electrokinetic charges: Distinctions and juxtapositionings. *Colloids and Surfaces A: Physicochemical and Engineering Aspects*, **376**, 2–8.

Lyklema J. & Minor M. (1998) On surface conduction and its role in electrokinetics. *Colloids and Surfaces A: Physicochemical and Engineering Aspects*, **140**, 33–41.

Ma C. & Eggleton R.A. (1999) Cation exchange capacity of kaolinite. *Clays and Clay Minerals*, **47**, 174–180.

Minor M., van Leeuwen H.P. & Lyklema J. (1998a) Low-frequency dielectric response of polystyrene latex dispersions. *Journal of Colloid and Interface Science*, **206**, 397–406.

https://doi.org/10.1180/claymin.2017.052.3.02 Published online by Cambridge University Press

Minor M., van der Linde A.J. & Lyklema J. (1998b) Streaming potentials and conductivities of latex plugs in indifferent electrolytes. *Journal of Colloid and Interface Science*, **203**, 177–188.

O'Brien R.W. & Rowlands W.N. (1993) Measuring the surface conductance of kaolinite particles. *Journal of Colloid and Interface Science*, **159**, 471–476.

O'Brien R.W. & Ward D.N. (1988) The electrophoresis of a spheroid with a thin double layer. *Journal of Colloid and Interface Science*, **121**, 402–413.

Rasmusson M., Rowlands W.N., O'Brien R.W. & Hunter R. (1997) The dynamic mobility and dielectric response of sodium bentonite. *Journal of Colloid and Interface Science*, **189**, 92–100.

Revil A. (2012) Spectral induced polarization of shaly sands: Influence of the electrical double layer. *Water Resources Research*, **48**, 1–23.

Revil A. (2014) Comment on: On the relationship between induced polarization and surface conductivity: Implications for petrophysical interpretation of electrical measurements. *Geophysics*, **79**, X1–X10.

Rouquerol J., Avnir D., Fairbridge C.W., Everett D.H., Haynes J.H., Pernicone N., Ramsay J.D.F., Sing K.S. W. & Unger K.K. (1994) Recommendations for the characterization of porous solids. *Pure and Applied Chemistry*, **66**, 1739–1758.

Rowlands W.N. & O'Brien R.W. (1995) The dynamic mobility and dielectric response of kaolinite particles. *Journal of Colloid and Interface Science*, **175**, 190–200.

Schofield R.K. & Samson H.R. (1954) Flocculation of kaolinite due to attraction of oppositely charged crystal faces. *Discussions of the Faraday Society*, **18**, 135–154.

Stanjek H. & Künkel D. (2016) CEC determination with Cu-triethylenetetramine: recommendations for improving reproducibility and accuracy. *Clay Minerals*, **51**, 1–18.

Swartzen-Allen S.L. & Matijević E. (1974) Surface and colloid chemistry of clays. *Chemical Reviews*, **74**, 385–400.

Thommes M., Kaneko K., Neimark A.V., Olivier J.P., Rodriguez-Reinso F., Rouquerol J. & Sing S.W. (2015) Physisorption of gases, with special reference to the evaluation of surface area and pore size distribution (IUPAC Technical Report). *Pure and Applied Chemistry*, **87**, 1051–1069.

Vasconcelos I.F., Bunker B.A. & Cygan R.T. (2007) Molecular dynamics modeling of ion adsorption to the basal surfaces of kaolinite. *Journal of Physical Chemistry C*, **111**, 6753–6762.

Weber C. & Stanjek H. (2012) Development of diffuse double layers in column-wicking experiments: Implications for pH-dependent contact angles on quartz. *Journal of Colloid and Interface Science*, **387**, 270–274.

Weber C., Heuser M., Mertens G. & Stanjek H. (2014) Determination of clay mineral aspect ratios from conductometric titrations. *Clay Minerals*, **49**, 17–26.

Weiss A. (1959) Über das Kationenaustauschvermögen der Tonminerale. III Der Kationenaustausch bei Kaolinit. *Zeitschrift für anorganische und allgemeine Chemie*, **299**, 92–120.

Weller A., Slater L. & Nordsiek S. (2013) On the relationship between induced polarization and surface conductivity: Implications for petrophysical interpretation of electrical measurements. *Geophysics*, **78**, D315–D325.

White L.R. (1982) Capillary rise in powders. *Journal of Colloid and Interface Science*, **90**, 536–538.

Zhou Z. & Gunter W. (1992) The nature of the surface charge of kaolinite. *Clays and Clay Minerals*, **40**, 365–368.

https://doi.org/10.1180/claymin.2017.052.3.02 Published online by Cambridge University Press